Supporting Information

Plasmonic Crystals for Strong Light-Matter Coupling in Carbon Nanotubes

Yuriy Zakharko[*]*, Arko Graf, and Jana Zaumseil*[*]

Institute for Physical Chemistry, Universität Heidelberg, D-69120 Heidelberg, Germany

Corresponding Authors

* E-mail: yuriy.zakharko@pci.uni-heidelberg.de

* E-mail: zaumseil@uni-heidelberg.de

1. METHODS

Sample fabrication, characterization and theoretical analysis.

2. RESULTS

1. Methods

SWCNTs dispersion preparation. (6,5) SWCNTs were prepared from CoMoCAT® raw material (diameter 0.7–0.9 nm, >93 % semiconducting SWCNT, 773735 Sigma Aldrich, Lot #14J017A1). Poly[(9,9-dioctyluorenyl-2,7-diyl)-*alt-co*-(6,6'-{2,2'-bipyridine})] (PFO-BPy, American Dye Source, M_W = 34 kg/mol) was dissolved in toluene (2 g/L) before adding 1.5 g/L CoMoCAT and applying sonication using a bath sonicator for 50 min. During dispersion in an ultrasonic bath (Bandelin Sonorex Digitec DT 102 H) the temperature was kept between 15 °C and 25 °C. Sonication was followed by centrifugation at 60,000 g (Beckman Coulter Avanti J26XP centrifuge) for 1 h. The supernatant was collected and the pelleted material was reused for repetitive dispersion with fresh polymer. (6,5) SWCNTs were enriched by pelletizing the monochiral dispersion by ultracentrifugation (Beckman Coulter OptimaMax XP table-top) at 284,600 g for 20 h. The resulting pellet was redispersed in a small volume of toluene.

Sample fabrication. Nanodisk arrays on glass substrates were fabricated by electron-beam lithography (EBL) with a Raith 150 system (Raith GmbH) as described previously[1]. SWCNT films were produced by drop-casting (10 µl drops one, three or seven times) of the highly concentrated toluene dispersion of (6,5) SWCNTs onto the substrates. Samples were finalized by spincoating a toluene solution (20 g/L) of poly(methyl methacrylate) (PMMA) (M_W=350000, Sigma Aldrich) at 1000 rpm leading to an SWCNTs/PMMA layer of 250-350 nm (depending on the amount of SWCNTs). For reference samples without SWCNTs only the PMMA layer was spincoated. The reported thickness of SWCNT and PMMA films was measured at different points by atomic force microscopy (AFM, Bruker Dimension Icon) in tapping mode and averaged.

Optical characterization. The absorption spectra of drop-cast SWCNT layers were acquired with a Varian Cary 6000i absorption spectrometer. The photoluminescence-excitation map was obtained by excitation of the SWCNT film with a wavelength tunable (1 nm step with laser-line tunable filter, Fianium Ltd.) output of a supercontinuum laser source (WhiteLase SC400, Fianium Ltd.) and detection with an Acton SpectraPro SP2358 spectrometer (grating 150 lines/mm) and a liquid nitrogen cooled InGaAs line camera (PI Acton OMA V:1024 1.7). The obtained signal was wavelength calibrated for sensitivity of the detection system and incident laser power (measured with a calibrated silicon photodiode power sensor).

For room temperature reflectance and photoluminescence (PL) spectroscopy, a collimated white light source or laser beam (λ=640 nm; continuous wave power 10 mW, OBIS, Coherent Inc.) was passed through a 50:50 beam-splitter and focused on the sample with a ×100 near IR objective with 0.8 numerical aperture. The spot size was about 1.5 µm and the effective angle of incidence/detection was ±50°. The back-focal plane of the objective was imaged via Fourier optics and a tube lens onto the entrance slit of a spectrometer (IsoPlane SCT-320, Princeton Instruments) equipped with cooled 2D InGaAs camera (640×512 pixels NIRvana 640ST,

Princeton Instruments). An additional polarizer was placed in front of the spectrometer to select transverse-electric (TE) or transverse-magnetic (TM) light polarization. Scattered laser light was blocked by a long pass filter with an 850 nm cutoff wavelength. The reflectivity was defined as the difference between signals from regions on the sample with and without plasmonic crystals divided by the measured spectrum of the lamp.

Simulations. 3D finite-difference time-domain (FDTD) simulations were performed using commercial software (FDTD Solution v8.15.697, Lumerical Solutions Inc., Canada) according to the approach discussed previously[1]. Briefly, for the calculation of the local plasmon resonance of a single nanodisk (Supporting Information Figure S3) a uniform mesh size of 1 nm (X, Y and Z-directions) was used in the region with steep variation of the dielectric function (X×Y×Z=200×50×200 nm^3 around a 25 nm high elliptical 160×180 nm gold nanodisk). Outside of these regions the grid was defined by the auto non-uniform mesh technique. The nanodisk was placed on the glass substrate and covered by 250 nm PMMA layer (n=1.5 for both). The optical constants of gold were taken from Johnson and Christy[2]. To reduce computational resources and time, we took advantage of the symmetric/antisymmetric boundary conditions. The incoming plane wave was injected normal to the surface and polarized along short or long axis of the elliptical gold nanodisk. The calculated difference between power entering and leaving the box power monitor around ND is used to deduce the absorption spectrum and thus position of the local plasmon resonances.

The field intensity enhancement profiles in Figure 1b were calculated as a ratio of the field intensity from the three 2D profile monitors (X-Y, X-Z and Y-Z planes) with and without gold ND (on a glass substrate covered by 450 nm PMMA layer, and arranged in the infinite square array defined by the 670×670 nm^2 periodic boundary conditions). Here, a uniform mesh size of 2 nm (X, Y and Z-directions) was used over the whole PMMA layer, i.e. X×Y×Z= 670×450×670 nm^3 region.

For the volume-averaged field intensity enhancement (Supporting Information Figure S6) the electromagnetic fields were recorded with a 3D monitor (a uniform mesh size of 3 nm (X, Y and Z-directions) X×Y×Z=670×(100/200/300)×670 nm^3 enclosing ND and top layer). Field intensity enhancement $|E_z/E_0|^2$ was calculated for a plane wave injected normal to the surface (Z-polarized) by averaging values from the 3D monitor excluding values of cells/positions of gold and dividing by the values of the same structure but without nanodisk.

Coupled-oscillator fitting routine. The dispersion properties of the surface-lattice resonances (SLRs) were fitted to the eigenvalues of the effective Hamiltonian separately for the TE and TM-polarized signal:

$$H_{SLR} = \begin{pmatrix} E_{LPR} & V_{RA1} & V_{RA2} \\ V_{RA1} & E_{RA1}(\theta) & V_{RA1-RA2} \\ V_{RA2} & V_{RA1-RA2} & E_{RA2}(\theta) \end{pmatrix}$$

, where spectral positons of the local plasmon resonance E_{LPR} for TE and TM were estimated from the FDTD simulations, 1.333 and 1.377 eV, respectively (see Figure S3). The off-diagonal V_{RA1}, V_{RA2}, $V_{RA1\text{-}RA2}$ coupling strengths were set as the fitting parameters and correspond to the coupling of the LPRs to the corresponding Rayleigh anomalies (RAs).

For the detection plane at φ=0 relatively to the symmetry of periodic arrays the uncoupled dispersion curves for the RAs $E_{RA1}(\theta)$ and $E_{RA2}(\theta)$ for TE (+1,0) and (-1,0) RAs are of the form:

$$E_{TE,(\pm 1,0)}(\theta) = \frac{h \cdot c}{a \cdot (n \mp \sin(\theta))}$$

While for the TM (0,±1) RAs:

$$E_{TM,(0,\pm 1)}(\theta) = \frac{h \cdot c}{a \cdot \sqrt{(n^2 - \sin(\theta)^2)}}$$

, where $h \cdot c$ is a product of the Planck constant and the speed of light, a is the array pitch and n is the refractive index of environment.

For the detection plane at φ=π/4 the uncoupled dispersion curves for the TE and TM-polarizations are the same, and $E_{RA1}(\theta)$ and $E_{RA2}(\theta)$ for (+1,0)/(0,+1) and (-1,0)/(0,-1) RAs are:

$$E_{TE/TM,(\pm 1,0)/(0,\pm 1)}(\theta) = \frac{h \cdot c}{a/\sqrt{2} \cdot (\sqrt{2 \cdot n^2 - \sin(\theta)^2} \mp \sin(\theta))}$$

2. Results

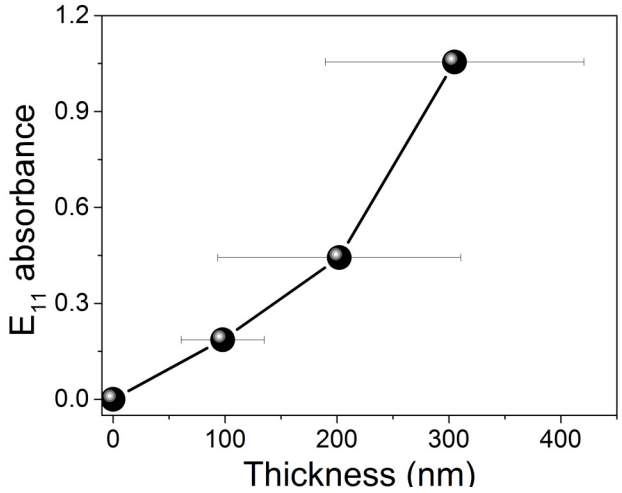

Figure S1. Dependence of SWCNT layer absorbance at E_{11} (λ=1000 nm) on film thickness, error bars indicate measured thickness variation over sample.

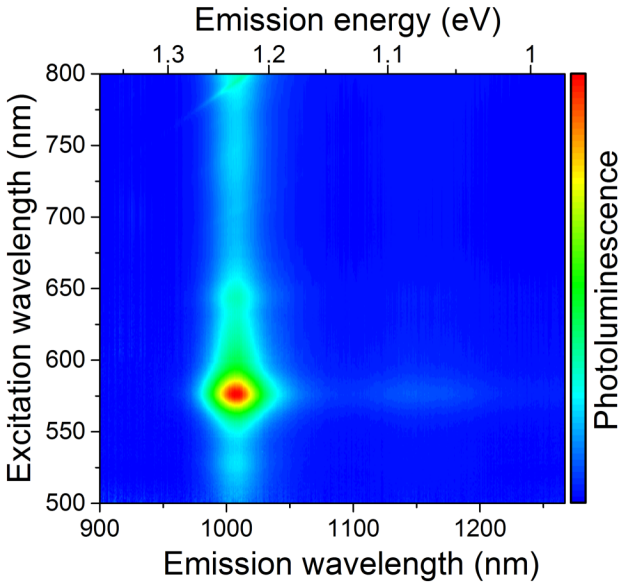

Figure S2. Photoluminescence excitation map of (6,5) SWCNT layer showing no other emitting SWCNT species.

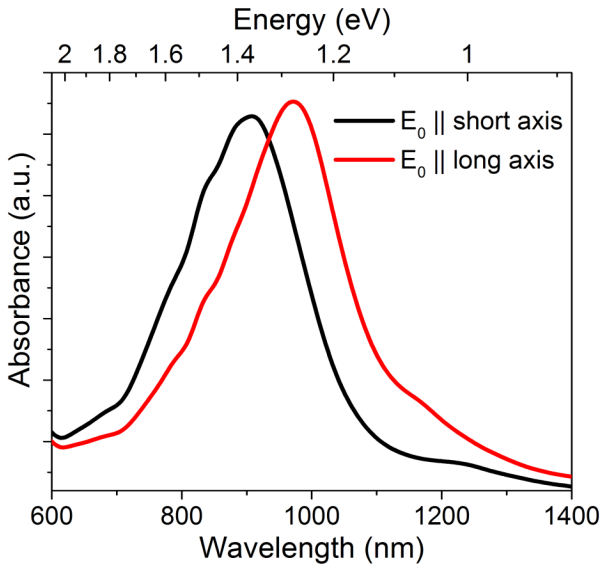

Figure S3. Local plasmon resonances of elliptical gold nanodisk. FDTD-simulated absorption spectra of elliptical (160×180 nm) gold nanodisk in dielectric environment with n=1.5 along short (black) or long (red) axis reveal slight changes in spectral position of local plasmon resonance.

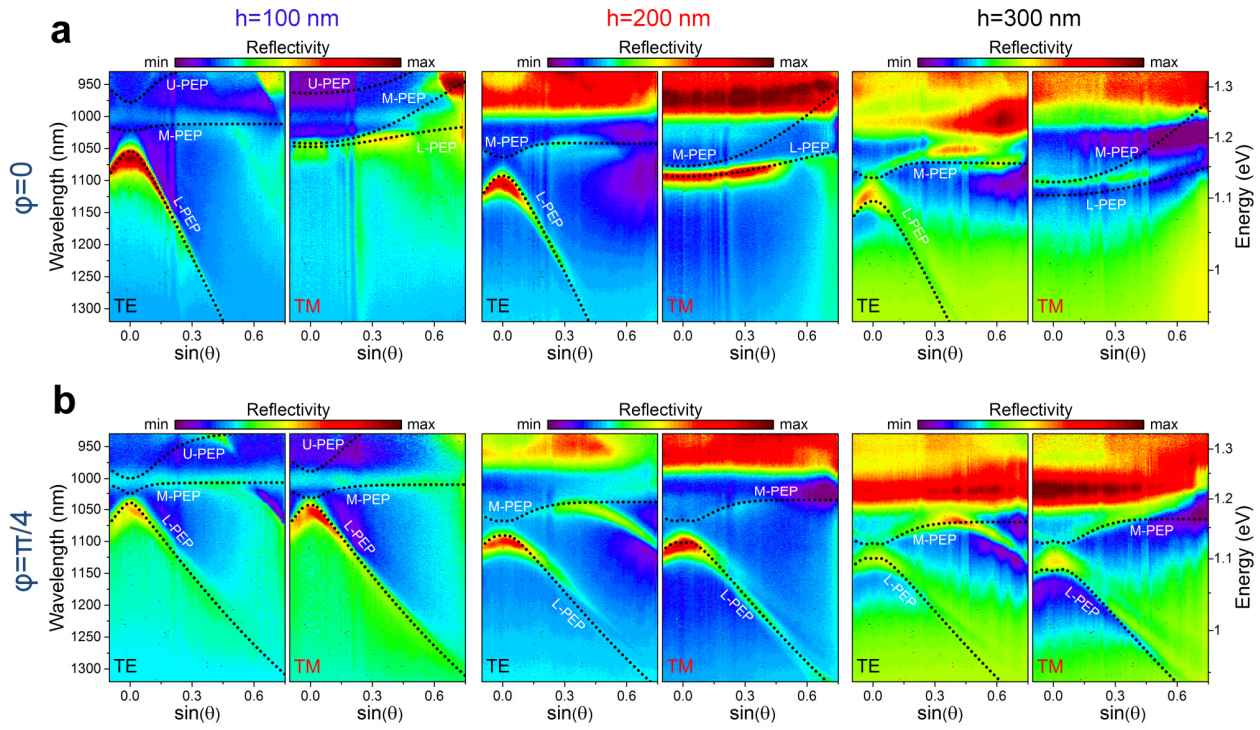

Figure S4. Angle- and polarization-resolved reflectivity spectra for samples with increasing SWCNTs layer thickness (from left to right) and for **(a)** φ=0 and **(b)** φ=π/4. Plasmon-exciton polariton dispersion curves (U-/M-/L-PEPs) were obtained from the fit of the PL results (black dotted lines) and show reasonably good correlation. For the sample in **(b**, right**)** deviations are caused by the large variation of the SWCNTs layer thickness and thus differences in coupling strength for two different points of PL and reflectivity measurements.

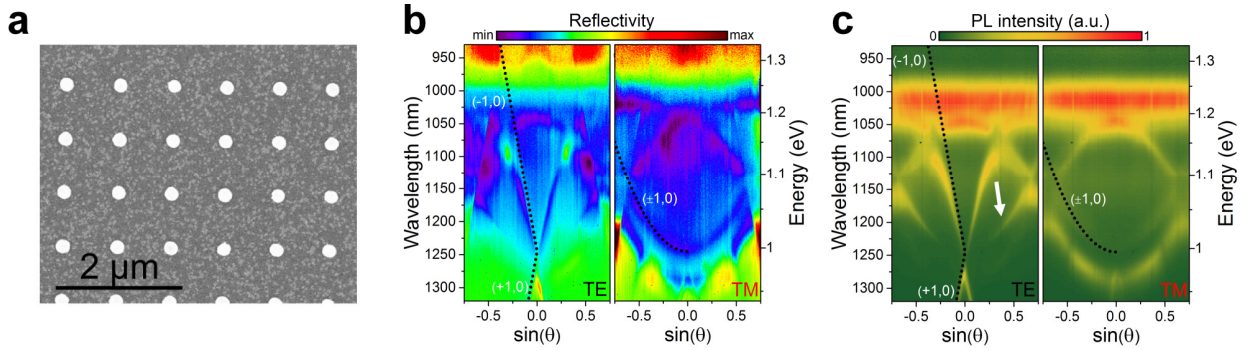

Figure S5. Representative results for a sample with a pitch of 830 nm. **(a)** Scanning electron micrograph of periodic array of gold nanodisks (830 nm pitch and diameter 220 nm). Angle- and polarization-resolved **(b)** reflectivity and **(c)** PL spectra for a sample with a 300 nm SWCNTs layer at detection angle φ=0. (±1,0) and (±0,1) Rayleigh anomalies defining the spectral features are shown as black dotted lines. The secondary TM-like feature in TE plot is indicated with a white arrow.

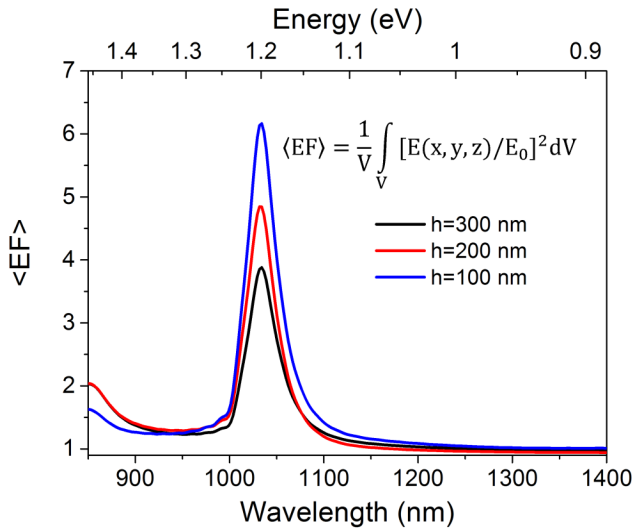

Figure S6. 3D-FDTD calculation of local field enhancement. Calculated volume-averaged field intensity enhancement around gold nanodisk (diameter 170 nm) in a periodic array over layer of 670x670 nm^2 area and 100 (blue line), 200 (red) and 300 nm (black) height.

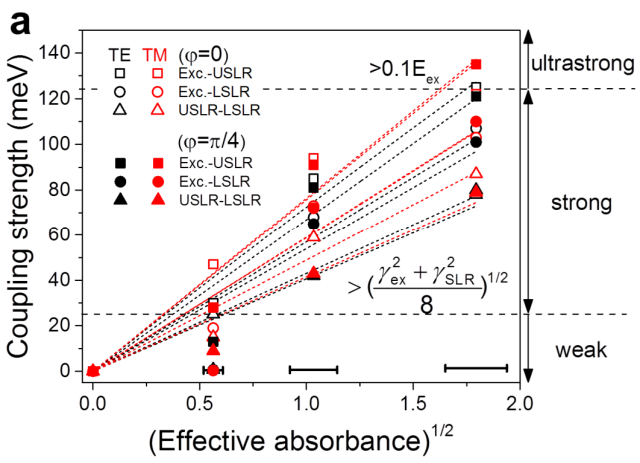

b

TE/TM	thickness (nm) /(eff. abs.)$^{1/2}$	100/0.56	200/1.03	300/1.79
φ=0 (meV)	Exc.-USLR	30/47	85/94	125/122
	Exc.-LSLR	0.4/19	68/73	107/103
	USLR-LSLR	25/15	43/59	78/87
φ=π/4 (meV)	Exc.-USLR	13/28	81/91	121/135
	Exc.-LSLR	0.6/0.3	65/72	101/110
	USLR-LSLR	0.7/9	42/43	80/79

Figure S7. Transition from weak to ultrastrong coupling regime. **(a)** Coupling strength between excitons and surface lattice resonances as a function of the square root of the effective absorbance (i.e. taking into account the E_{11} absorbance and volume-averaged coupling efficiency) for the TE (black) and TM (red) polarized light and detection at φ=0 (open symbols) and φ=π/4 (solid). Transition regions of weak-to-strong and strong-to-ultrastrong coupling regimes are indicated with horizontal dashed lines. Least squares fit to the values are presented with dotted lines. **(b)** Table view of the corresponding coupling strength values.

REFERENCES

(1) Zakharko, Y.; Graf, A.; Schießl, S. P.; Hähnlein, B.; Pezoldt, J.; Gather, M. C.; Zaumseil, J. *Nano Lett.* **2016**, *16*, 3278–3284.

(2) Johnson, P. B.; Christy, R. W. *Phys. Rev. B* **1972**, *6*, 4370–4379.